Thin Flexible RF Energy Harvesting Rectenna Surface with a Large Effective Aperture for Sub-μW/cm^2 Powering of Wireless Sensor Nodes

Mahmoud Wagih, *Member, IEEE*, and Steve Beeby, *Fellow, IEEE*

***Abstract*—The DC power collected by Radio Frequency Energy Harvesting (RFEH) absorbing surfaces is limited by their physical aperture. Here, a compact, conformable, and ultra-thin sub-1 GHz large-area RFEH surface is proposed based on electrically-small (ka=0.58) "wire-type" rectenna elements, with an effective area exceeding its physical aperture size. Using optimized large-signal complex source tuning, the rectifiers achieve up to 36% measured Power Conversion Efficiency (PCE) at −20 dBm. The proposed 15 cm-diameter six-element array generates a 27.5 μW at 1 V output from a 0.17 μW/cm^2 incident power density across a 40 kΩ load. Owing to its series connection, the voltage output is boosted and the load resistance-dependence is suppressed enabling over 60% of the maximum RF-to-DC PCE to be preserved for loads between 7 and 100 kΩ, with an area-normalized Figure-of-Merit nearly 100% higher than previous arrays. The proposed array is integrated with a commercial DC-DC converter and demonstrated powering a Bluetooth Low Energy (BLE) wireless sensor node from an unprecedented incident power density of 0.25 μW/cm^2. A practical demonstration using a commercial 3 W 915 MHz Powercast source is presented showing an 11 m operation range with a 1 V output, and illustrating the impact of polarization mismatch on the proposed array.**

***Index Terms*—Antennas, Battery-less Sensor Nodes, Energy Harvesting Surface, Metamaterials, Metasurfaces, Rectennas, Rectifiers, RFID, Wireless Power Transfer.**

I. Introduction

LARGE-AREA Radio Frequency (RF) Energy Harvesting (EH) surfaces, such as large rectenna arrays, have recently emerged as a solution to maximize the DC power output from low incident power densities [1], compared to RF harvesters based on individual rectennas [2]. In long-range Wireless Power Transmission (WPT) and RFEH for Internet of Things (IoT) and Internet of Everything (IoE) applications, it is desirable to harvest as much power as possible, efficiently, at very low power levels such as sub-1 μW/cm^2 power densities [3]–[6], which translates to operation ranges in excess 10 m based, constrained by Equivalent Isotropically Radiated Power (EIRP) regulations, as well as enabling ambient RFEH [3].

This work was supported by the UK Royal Academy of Engineering and the Office of the Chief Science Adviser for National Security under the UK Intelligence Community Post-Doctoral Research Fellowship programme. S. Beeby was supported by the UK Royal Academy of Engineering under the Chairs in Emerging Technologies scheme. (*Corresponding author: Mahmoud Wagih*)

M. Wagih is with the James Watt School of Engineering, University of Glasgow, G12 8QQ (email: Mahmoud.Wagih@IEEE.org)

S. Beeby is with the School of Electronics and Computer science, University of Southampton, Southampton, SO17 1BJ, U.K.

Digital Object Identifier: .

A myriad of RFEH surfaces have been reported including broadband surfaces [1], [7], polarization-insensitive surfaces [8], and full-wave rectifying surfaces [9]. Broadband RFEH surfaces have been reported based on spiral antenna elements operating up to 18 GHz [10]. A screen-printed array operating between 2 and 4 GHz has recently been reported on a textile substrate with nearly 50% efficiency (normalized to the physical area) for wearable energy harvesting [11], but only from power densities exceeding 100 μW/cm^2 which require nearly 47 dBm EIRP to enable a 1 m range of operation. Recently, a Fabry-Perot-based 3D absorbing array was demonstrated with an effective area larger than its physical size and high-efficiency at low power levels [12]. However, the array still required a large RF input over 1 μW/cm^2, and relied on a 3D structure with a height around 4 cm (λ/8.5).

To date, from a real-world application perspective, the reported large-area RFEH arrays have several limitations:

1) All reported 2D RFEH surfaces had an effective receiving aperture that is smaller than their physical size [7]–[14], highlighting the need for an improved antenna-rectifier co-design based on electrically-small elements.
2) None of the existing single-layer RFEH surfaces has been reported with a high efficiency (>20%) from power densities under 1 μ W/cm^2 [7]–[14], unlikely to be found in real-world applications beyond a few meters based on EIRP limits.
3) Most reported RFEH surfaces were implemented using costly, rigid, and double-sided RF laminates [7]–[10], [12]–[14], which does not satisfy the requirements of inexpensive IoT systems, especially when scaled to large-surface and high-volume applications.
4) When an RFEH surface was reported using inexpensive printed materials [11], its RFEH efficiency was limited to 32% for inputs exceeding 100 μW/cm^2, demonstrating that existing RFEH surface designs require the low-loss dielectrics and conductors to operate efficiently.

On the other hand, many efforts dealing with single rectennas have demonstrated sub-1 μW/cm^2 power harvesting using antennas on inexpensive substrates such as FR4 [4], 3D printed dielectrics [15], paper [16], polyimide/Kapton [17]–[19] and textiles [20]. Moreover, the Power Conversion Efficiency (PCE) of individual rectennas, based on complex-conjugate antenna-based matching [17], [19], [21], often outperforms that of their surface counterpart, especially at low power densities. As such, there is a need for a high-PCE, inexpensive,

and large-effective aperture RFEH surface to be realized using electrically-small elements.

In this paper, we present for the first time a planar RFEH array with an effective aperture larger than its physical size, achieving an unprecedented sub-1 μW/cm^2 sensitivity while being implemented on an inexpensive single-layer ultra-thin flexible film. In Section II, we lay out the foundation of high-area-efficiency RFEH using electrically-small rectennas. Section III then presents the practical design and integration of a sub-1 GHz rectenna element, based on our previous antenna design in [19], for the large-area array, as well as detailing the power-combining strategy. Section IV presents the rectenna surface experimental characterization, a demonstration powering a real-world sensor node from a sub-μW/cm^2 power density, and a comparison with prior works.

II. Electrically-Small Large-Area RFEH

With the recent research interest in receiving antennas as opposed to characterizing receivers solely based on reciprocity, the effective aperture (i.e. area) can be used to describe the way tightly-coupled receiving antennas intercept an incident Poynting vector [22]. Arrays are often designed for uniform excitations with balanced phases and RF combining. As such, the effective receiving aperture of individual elements drops significantly when the elements' apertures overlap [22]. However, in RFEH, large-area arrays are based on DC combining [10], and hence the array factor is not of paramount importance, as each element is terminated using the rectifier.

At a fixed distance d for a wireless power source, the incident Poynting vector (power density) is given by

$$S(\theta,\phi) = \frac{P_{\mathrm{TX}} G_{\mathrm{TX}}(\theta,\phi)}{4\pi d^2}, \tag{1}$$

where $P_{\mathrm{TX}}G_{\mathrm{TX}}$ are limited in real-world applications by the EIRP regulations.

For a receiving antenna, the antenna's collecting area, i.e. effective aperture, is given by

$$A_{\mathrm{eff.}} = \frac{G\lambda^2}{4\pi}, \tag{2}$$

where G is the antenna's gain, often obtained through the reciprocity of the transmit and receive gains [23]. However, in the case of an electrically-small antenna, A_{eff}, is often larger than the antenna physical size, which is highly-desirable in RFEH applications [24], [25]. For a rectenna to be considered electrically small, it needs to satisfy

$$ka = \frac{2\pi}{\lambda} \times a < 1 \tag{3}$$

where k is the angular wavenumber and a is the minimum radius of a sphere which fully encloses the antenna [26].

Therefore, when designing a "compact" rectenna, a small antenna with a high gain is highly desirable [4], [24], [25]. Should the small rectenna be adopted as the element within a large RFEH surface, with DC combining, the array will be expected to, in turn, exhibit an $A_{\mathrm{eff.}}$ exceeding its physical area. Fig. 1 (a) and (b) visualize the power reception of an aperture-type microstrip antenna and a small wire-type antenna, respectively, through a 2D Poynting vector sketch

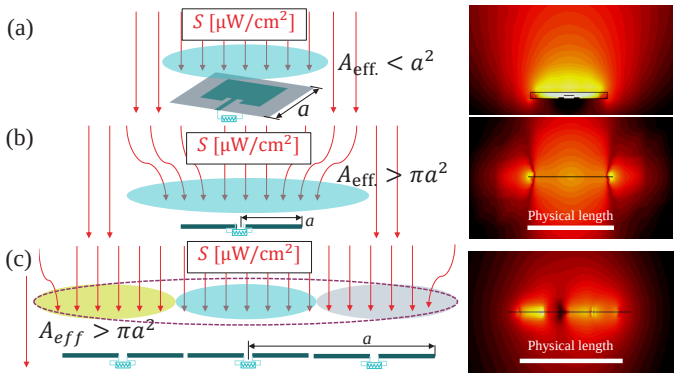

Fig. 1. 2D illustration of the power collection mechanism, based on [22], and simulated Poynting vector of: (a) an aperture-type microstrip antenna; (b) a wire-type dipole; (c) a three-element array based on tightly-coupled dipoles.

[22], as well as the simulated Poynting vector surrounding the antenna in CST Microwave Studio. Fig. 1(c) shows the predicted response for a three-element array, where the three elements are closely coupled with semi-overlapping effective areas.

As illustrated in Fig. 1(b), a small antenna can have an effective harvesting aperture larger than its physical radius, a concept which has previously been used to design miniaturized single-element rectennas [24]. Moreover, we have previously shown that when two wire-type rectenna of approximately the same gain, but significantly different footprints, were exposed to the same S, the harvested energy was the same [25]. The concept of co-locating multiple energy harvesting antennas in the same space has been proposed in [27], showing the potential for minor improvements in the DC power output, despite the antennas being fully overlapped.

Nevertheless, most RFEH surfaces to date were based on near-perfect absorbers with an effective collecting aperture that approaches their physical size, but does not surpass it. This has led to many studies calculating the "PCE" of their RFEH surfaces using the physical size [8], [11], [13], [14]. Should this "PCE" definition be used with an antenna whose $A_{\mathrm{eff.}}$ exceeds its physical size, such as [24], it will lead to a non-physical PCE exceeding unity (>100%).

In this work, we calculate the PCE as

$$\mathrm{PCE} = \frac{P_{\mathrm{DC}}}{P_{\mathrm{RF}}} = \frac{P_{\mathrm{DC}}}{S A_{\mathrm{eff.}}}, \tag{4}$$

based on the power received by the antenna P_{RF}. In line with previous works and to demonstrate the significant improvement achieved by the proposed array, a "Figure of Merit" (FoM) is defined based on the previous definition used to calculate the efficiency of RFEH surfaces as

$$\mathrm{FoM} = \frac{P_{\mathrm{DC}}}{S_{\mathrm{CoP}} . A_{\mathrm{physical}}} \tag{5}$$

where A_{physical} is the antenna/array's physical footprint (area), and S_{CoP} is the co-polarized component of the illumination. Therefore, this "FoM" enables the evaluation of a rectenna's PCE and overall compactness, in direct comparison with recent RFEH surfaces. On the other hand, the PCE calculation based on $A_{\mathrm{eff.}}$ in (4) ensures the rectifier's efficiency is

conservatively calculated based on the received power. This "FoM" definition has been widely used in previous works as the "PCE" [9], [12]–[14], and has been usually below 100%, except when a fabry-perot resonant structure was used in [12].

III. Rectenna and Array Design

Distinguishable from widely-spaced rectenna arrays, the proposed array aims to demonstrate the merits of ultra-low-power energy harvesting using tightly-coupled rectenna elements. To explain, one of the earliest planar and conformable rectenna arrays reported by Brown and Triner exhibited one of the highest efficiency rectennas to date, at 2.4 GHz, using a large-area array etched on a flexible substrate, where the elements were widely-spaced [28]. On the other end of the spectrum, Mi *et al.* proposed the use of overlapped antennas, deployed in the same space as an individual antenna, showing minimal DC power output gains [27]. Therefore, the proposed array targets the gap between widely-spaced ($> \lambda/2$) elements [28], and fully-overlapped rectennas [27].

The proposed rectenna and its array are designed to operate in the 915 MHz band. From 902 to 928 MHz, the FCC permits a 36 dBm (4 W) EIRP with 6 dBi antenna gain. In Europe, the EU EN 302 208 standard permits RFID readers to have an EIRP of 4 W at 915 MHz, which can be used as a power source for sub-1 GHz RF energy harvesters. As the array is aimed at low-cost pervasive IoT applications, a single-sided low-profile design is required. Furthermore, the implementation of the rectenna at a relatively low frequency reduces the conductor and dielectric losses in the antenna.

A. Single-Element Rectenna

To maintain a simple and scalable structure and eliminate the losses associated with lumped matching inductors [5], [16], antenna-rectifier co-design based on complex-conjugate matching is adopted in this work. A Folded Dipole Antenna (FDA) design with a scalable input impedance based on [19] is chosen as the first design step. The design in [19] features a small physical area, scalable input impedance, and a single-layer construction. However, the proposed surface-integration approach can be applied to any reported complex-impedance rectenna design in the literature such as Huygens dipoles [24], [29], narrow compact dipoles [17], as well as RFID antennas matched to their chip's rectifier [30]. Fig. 2(a) shows the layout and dimensions of the FDA element. The antenna is electrically small with ka=0.584 (based on a radius a=30.4 mm and k=19.16 at 915 MHz).

As the rectifier is aimed at sub-μW/cm^2 harvesting, the Skyworks SMS7630-079LF Schottky diode is chosen as the rectifying element for its ultra-low forward voltage ($0.04< V_F <0.14$ V) drop [31], [32], to maximize the PCE at low RF inputs [33]. The input impedance of the voltage doubler has been iteratively tuned in Keysight Advanced Design Systems using Harmonic Balance (HB) simulations to extract the input impedance to which the FDA will be scaled.

To enable simple modelling of the rectifier without the need for electromagnetic co-simulation, the layout from Fig. 2(b)

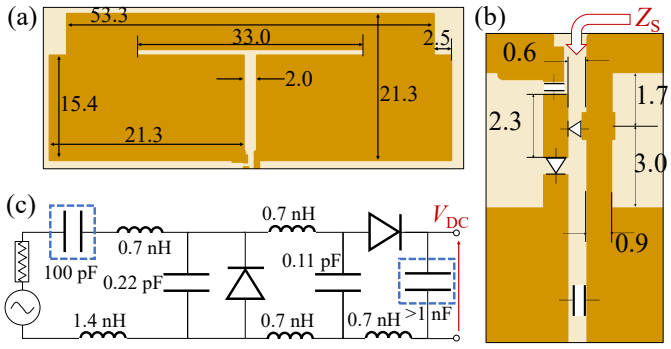

Fig. 2. The individual rectenna element: (a) the FDA geometry (dimensions in mm); (b) the rectifier's layout; (c) the rectifier's HB equivalent circuit model (enclosed capacitors indicate lumped components).

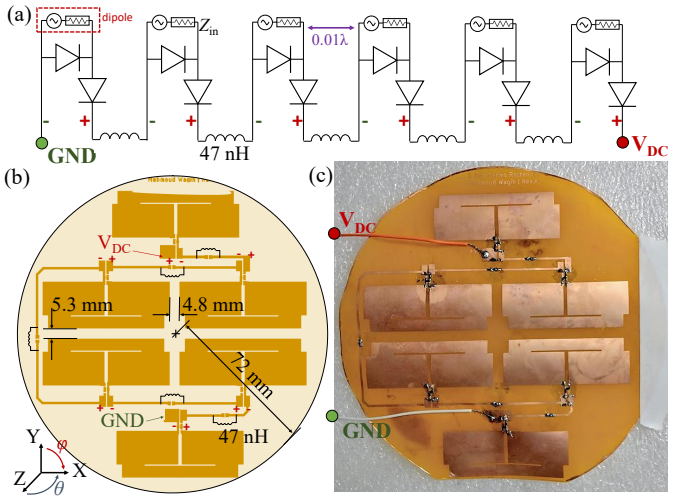

Fig. 3. The six-element flexible surface: (a) schematic of the power combining mechanism; (b) layout and dimensions; (c) and photograph.

was modeled as a loss-less transmission line using LC elements. Based on the coplanar strip capacitance and inductance per unit length [34], $L/\Delta z$=0.7 nH/mm and $C/\Delta z$=50 fF/mm were obtained based on ϵ_r=3.4 (for polyimide) and the dimensions of the traces. Fig. 2(c) shows the equivalent circuit model of the rectifier inclusive of the layout effects. The diodes in Fig. 2(c) include the packaging parasitic inductance and capacitance based on their datasheet values [5]. The capacitors enclosed by a dashed frame represent discrete lumped ceramic capacitors as opposed to distributed line capacitance.

B. Surface Design and Power Combining

To realize the RFEH surface, six FDA rectenna elements were closely spaced with <6 mm element spacing ($0.01\times\lambda$), as shown in Fig. 3. A DC summation network connects the array elements with RF-blocking 47 nH inductors added between each element. The presence of the inductors prevents the DC combining traces from creating spurious resonances which can shift the FDAs' impedances from their desired values. The inductors have a self-resonant frequency above 2 GHz, not to introduce additional variations to the FDAs'

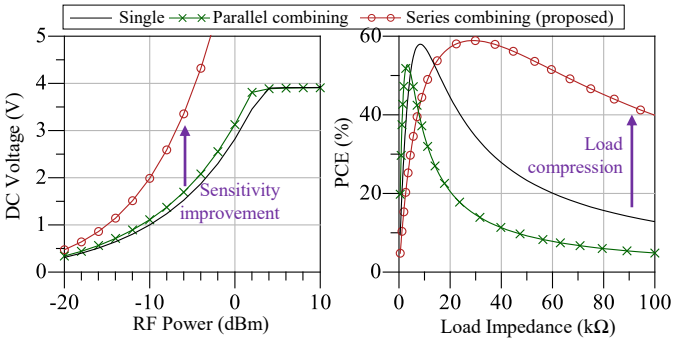

Fig. 4. Comparison of series and parallel combining for low-power RFEH: (a) DC voltage output across a high-impedance load; (b) load/PCE relation.

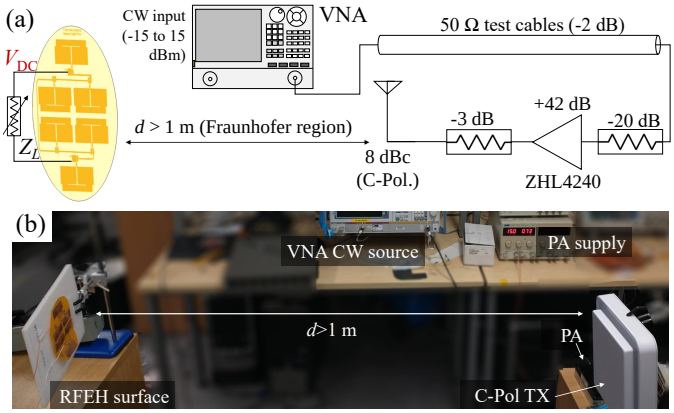

Fig. 5. Experimental setup: (a) block diagram; (b) photograph.

impedance. The DC-combining traces have a minimum width of 1 mm to minimize any additional series resistance.

The individual FDA cell and array were fabricated using photolithography on single-sided polyimide copper laminates. The polyimide and adhesive maintain a relative permittivity around 3.2 and tanδ=0.002 with a thickness around 40 µm. The copper thickness is 18 µm. This fabrication method has been widely used to realize flexible microwave and mmWave components with fine features and high conductivity [35]. Fig. 3(b) shows a photograph of the RFEH surface.

In most real-world RFEH applications, the output DC voltage of a rectifier is the obstacle hindering integration with an off-the-shelf Power Management Integrated Circuit (PMIC). Therefore, a series connection between the elements is chosen to boost the voltage output. A two-rectenna array is simulated in ADS (HB simulation) with series and parallel combining to illustrate the benefits of series voltage summation. Fig. 4(a) shows the voltage output across a high-impedance (50 kΩ) load for varying RF inputs, where the sensitivity improvement by the series connections is evident.

An additional advantage of the series connection in the proposed complex-conjugate surface is the resistive load compression. To explain, the input impedance of a rectifier is highly dependent on the load which limits its operation to a small range of load currents. Resistance compression through multi-path rectifiers with opposite phase responses has been widely used to suppress the influence of varying loads on the rectifier's efficiency [36], [37]. In Fig. 4(b), it can be seen that the effect of varying the load on the PCE was minimized in the series-connected array. This is validated experimentally against the single-cell rectenna in Fig. 11. While the rectifier's feed does not exhibit opposite phases, the observed response could be attributed to the high reactance-to-resistance ratio in the rectifier's source impedance which minimizes the influence of the load/current draw on $\Re\{Z\}$, as well as the absence of a "load" at the output of the first rectifier, which is directly connected to the second rectifier.

Unbalanced power inputs over a large array can lead to inefficiencies, with a minimum loss around 3% for six elements [38]. A potential problem that arises from connecting unbalanced rectifiers in series, which can reduce the overall DC output, is current reversal [32], with forward bias diodes often used to overcome this issue [39]. Nevertheless, this behavior is not expected in the proposed array as all elements will be illuminated by the same S resulting in a mostly balanced power distribution over the FDA elements. Therefore, only the inductors are used in this work, where their series resistance, at DC, is under 1 Ω compared to at least 5 Ω (along with the V_F drop) for commercial Schottky diodes.

IV. Surface Experimental Characterization

The proposed RFEH surface is characterized using a wireless source in the far-field at a distance of 1.2 m, satisfying the Fraunhofer far-field condition based on the transmitting and receiving antenna's maximum dimension under 30 cm. A circularly-polarized (CP) RFID patch, with a datasheet gain of 8 dBi, is connected to the output of a Mini-Circuits ZHL-4240+ 1 W Power Amplifier (PA). A Vector Network Analyzer (VNA) is configured to act as a Continuous Wave (CW) source feeding the PA; the VNA's power output was validated against an external signal generator. A CP source is used to ensure the measurements are not affected by polarization misalignment [40], [41]; in the direction of powering, i.e. θ=0°, the average axial ratio over all six elements is over 17 dB, showing that the arrays is predominantly linearly-polarized. The effect of linear polarization alignment in a multi-path environment is investigated in Section IV-E.

Fig. 5 shows the block diagram and photograph of the experimental setup. Due to the unavailability of an appropriate coupler to estimate the RF input to the CP antenna, the 41 dB gain of the PA was assumed to be linear across the full CW range investigated. The cable loss of 1 dB corresponds to the VNA/PA interconnect (a phase/amplitude-stable test cable), the losses in the adapters connecting the PA to the antenna were not included in the EIRP calculation, which results in a more conservative over-estimate of S at the rectenna's input.

A. Single-Element Rectenna Characterization

A rectenna element was characterized individually to establish a benchmark for the array's performance. A frequency and load sweep were first carried out; the optimum load and frequency were found to be 5 kΩ and 900 MHz respectively. Following the load and frequency sweeps, the CW input was swept to observe the rectenna's PCE for varying S. Fig. 6

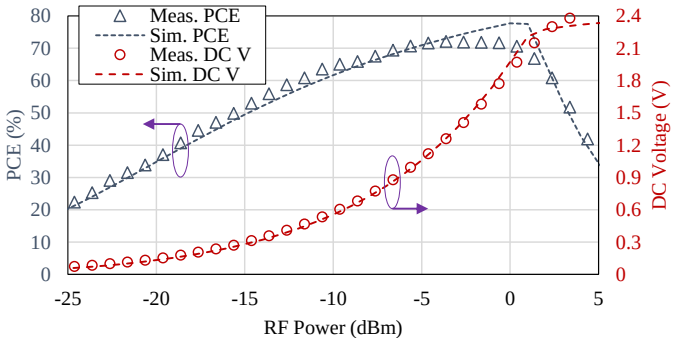

Fig. 6. Simulated (Z_S=50+jω35×10^{-9}Ω) and measured DC output and PCE of the individual rectenna at 900 MHz, a 5 kΩ load, and d=1.15 m.

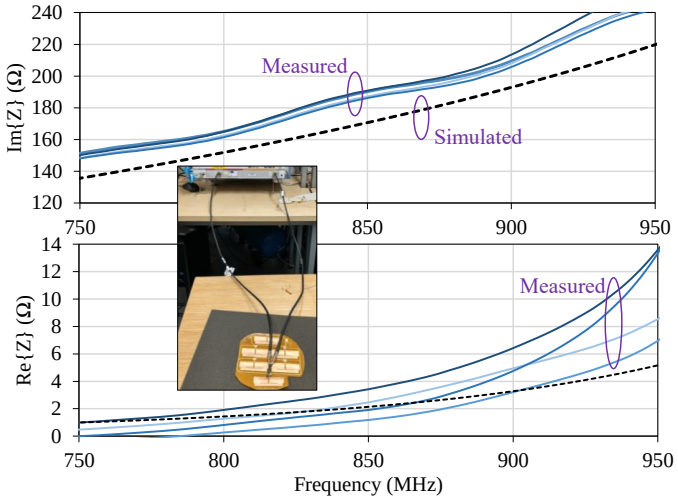

Fig. 7. Simulated (dashed) and measured (solid) input impedance of the individual elements in the FDA array; inset shows the measurement setup.

shows the simulated and measured PCE and DC voltage output across a 5 KΩ load, in close agreement. At −20 dBm, the rectenna achieves a PCE of 36%, in line with state-of-the-art rectennas [17], [32], [42], while keeping a relatively low optimum load impedance. The HB-simulated response was obtained using the circuit model in Fig. 2(c), with a source impedance of 50 Ω and a 35 nH inductor at 900 MHz.

The FDAs' input impedance Z_{in} was measured using a two-port VNA and a common-ground coaxial jig. The measured Z_{in} is shown alongside the simulated response in Fig. 7. The measured Z_{in} of the different array elements are mostly in line with each other as well as with the simulated response. $\Im\{Z_{in}\}$ is in line with the simulated optimum rectifier Z_{in} of 198 Ω at 900 MHz. The full-wave simulated and measured $\Re\{Z_{in}\}$ of the FDA is lower than the optimum $\Re\{Z_{in}\}$ ranging from 30 to 50 Ω. However, this did not affect the rectenna's DC output, as observed in Fig. 6, where the simulated response was obtained using a Z_{in}=40+j189 Ω.

B. Power Density Sweep

The DC output of the six-element surface was measured at d=1.2 at 920 MHz across its optimal load of 40 kΩ for varying S. To demonstrate that the array's $A_{\text{eff.}}$ exceeds its physical footprint, the FoM is calculated using (5) and the array's

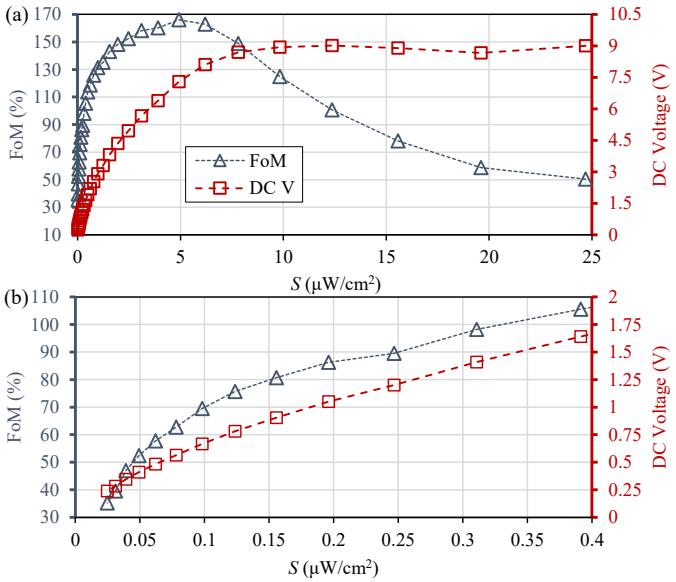

Fig. 8. Measured DC voltage output and FoM of the propsoed RFEH surface at 920 MHz: (a) over a wide S range; (b) the sub-0.5 μW/cm^2.

physical area of 162.8 cm^2; a FoM>100% will demonstrate that $A_{\text{eff.}}$ exceeds the physical footprint and maintains high rectifier PCE. Fig. 8 shows the FoM and DC voltage output of the array for varying S.

From Fig. 8(a), the peak FoM approaching 170% indicates that the array's effective collection area is nearly twice its physical size, as the rectifier's PCE is under 80% (as previously seen in Fig. 6). Observing Fig. 8(b), the surface generates a 1 V DC output (27.5 μW) from $S \approx 0.2$ μW/cm^2, demonstrating that the proposed RFEH surface being is the first to efficiently (FoM>50%) harvest a sub-1 μW/cm^2 S [1], [7], [8], [10], [11], [13], [14]; a detailed comparison is presented in Section IV-F.

For S <0.4 μ W/cm^2, the forward voltage losses of the rectifier limit the PCE; these approximately correspond to inputs under – 10 dBm in Fig. 6. When S exceeds 6 μW/cm^2, the low breakdown voltage of the SMS7630 limits the PCE hence degrading the FoM. However, such a high S can only be present at less than 2 m from an FCC-compliant 4 W EIRP source, and can be overcome by choosing a higher breakdown voltage diode. For S > 15 μW/cm^2, the sharp drop in the DC voltage output is attributed to the PA's gain compression reducing the EIRP as the CW input approaches its absolute rating.

Fig. 9 compares the DC power output of the six-element surface to that of the individual rectenna. Over nearly all S values investigated, the array offers at least a two-fold power gain over the single rectenna. For benchmarking, the optimally-matched (with Z_S=50+j198 Ω) individual rectenna's output was simulated alongside the six-element array (with the measured Z_S=8+j198 Ω). The simulated DC power output improvement by the six series-connected rectifiers was between 4 and 3.4× that of the single (matched rectifier).

This simulated power gain (3.4–4×) is however higher than the measured response, in Fig. 9, as it assumes that the

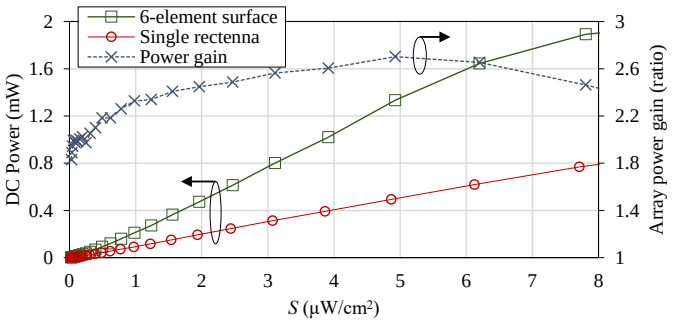

Fig. 9. Comparison of the DC power output of the single-element rectenna and the six-element tightly-coupled surface.

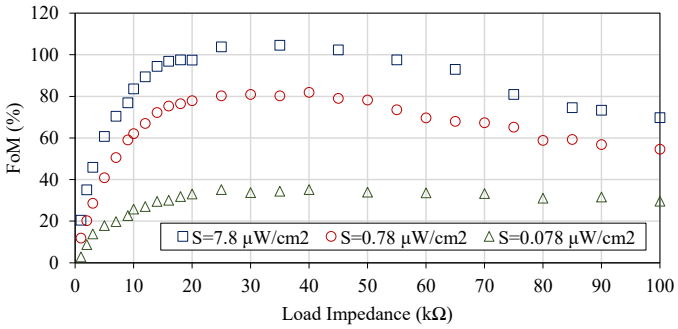

Fig. 10. Measured FoM for varying load impedances at 920 MHz.

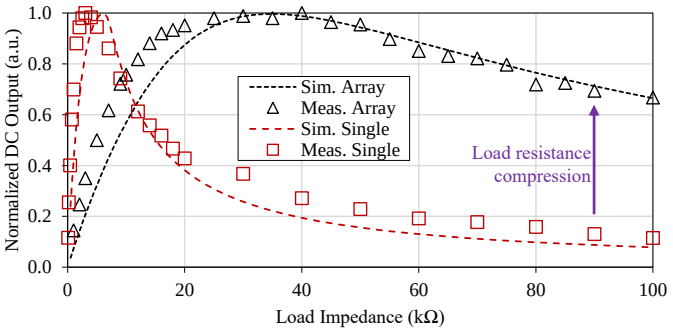

Fig. 11. Comparison of the surface and rectenna's PCE over varying load impedances, showing the resistive load compression.

individual elements in the array will receive the same amount of RF power as the single rectenna, which will not be the case due mutual coupling and overlapping effective areas. To explain, using (2) and the full-wave simulated directivity of the single rectenna of 2.0 dBi, $A_{\text{eff.}}$ of the individual rectenna is 141 cm^2, which is very comparable to the array's total physical area of 162.8 cm^2. This implies that the additional elements will have overlapping effective apertures reducing the power received by each element [22]. Therefore, using the measured power gain of 2.6× the single rectenna's output, and the simulated maximum gain of 4×, the area (i.e. aperture) efficiency of the six-element array could be conservatively estimated as 65% of the individual antenna's.

Nevertheless, the tightly-coupled surface still exhibits significant improvements over the individual rectenna, and previous arrays and surfaces [7]–[14], in the form of:

1) improving the 1 V sensitivity by over ten-fold, from S=1.93 μW/cm^2 (for the individual rectenna), to S=0.17 μW/cm^2;
2) resistance compression-like response, observed in Fig. 4(b), and further explored in the next sub-section;
3) maintaining an effective area nearly twice its physical footprint despite the tight coupling.

Therefore, the proposed array is justified compared to single-rectenna RFEH, especially when its inexpensive and simple construction is taken into consideration.

C. Load and Angle of Incidence Sweeps

The RFEH surface's output was connected to a decade resistor box and the load was swept from 100 Ω to 100 kΩ. The FoM of the array at different S across the variable loads is shown in Fig. 10. In the three S illuminations investigated, minimal changes are observed in the optimal load impedance. It can also be seen that the surface rectifiers' exhibit minimum sensitivity to the varying load impedance over a wider range. To explain, the single rectenna element maintains 80% or more of its peak DC power output for loads ranging between 2.5 and 8.6 kΩ, translating to a resistance ratio of 3.33:1. On the other hand, the proposed six-element array maintains 80% or more of its DC power output for loads ranging from 12 to 75 kΩ, i.e. 6.25:1 ratio, which demonstrates a 1.88× improvement over the single rectenna. The optimum load impedance shift to a high resistance, as the voltage output increases, is in line with previously-reported serially-connected rectennas [43].

The normalized DC output of the six-element surface and the single-element rectenna, in response to a varying load, is shown in Fig. 11. It can be seen that for a 10:1 load resistance ratio, the surface maintains at least 60% of its peak DC power output, while the single rectenna's output drops to around 10% of the maximum DC output. This response is in-line with previously reported resistance compression RFEH rectifiers [36], [37], both of which rely on separate matching networks with opposite phases and a single rectifier.

As the FDA is an omnidirectional low-directivity antenna, the surface is expected to maintain a wide angular coverage. The simulated elevation (XY plane) normalized patterns at φ=0° of the array elements are shown in Fig. 12(a). Experimentally, the RFEH surface was rotated around its XZ (elevation) plane, shown in Fig. 3, and its DC output was measured. Fig. 12(b) shows the measured DC output, in dBm, alongside the simulated gain pattern of the combined array. The elements' gains were combined under a simultaneous excitation. The discrepancy observed could be attributed to multi-path reflections, as the measurement was not carried out in an anechoic range, and inaccuracies in the positioning leading to the shifted main lobe. In Fig 12(c), it can be seen that the measured harvested angular DC power patterns exhibit minimal variations in response to changing the input power density.

While the individual rectenna elements are horizontally (H)-polarized, with a vertically (V) "cross"-polarized of around 6 dBi, the patterns of the antenna elements within the array ex-

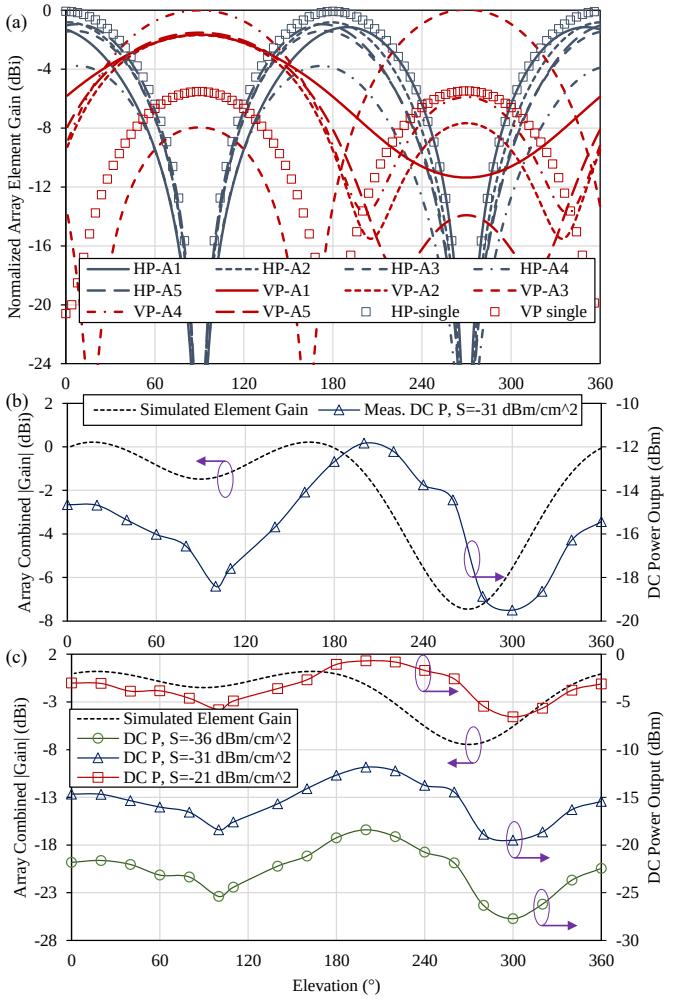

Fig. 12. The RFEH surface's radiation and DC collection patterns: the simulated XZ (φ=0°) patterns of each array element; (b) simulated combined array absolute gain along with the DC harvested power; (c) the effect of varying S on the DC power patterns at S=–31 dBm/cm^2.

hibit a high V-polarized component, as seen in Fig. 12(a). The observed low polarization-purity is attributed to the feeding network which includes vertical traces of comparable size to the radiators, closely coupled to the rectenna elements which leads to a higher V-polarized component. This is also evidenced by the stable "co" H-polarized component over all the array elements, whereas the "cross" V-polarized component is dependent on the position within the array. However, in the context of energy harvesting, a low-polarization purity is not a drawback, and has been considered a favorable property in ambient RF energy harvesting [42]. We demonstrate in Section IV-E that the low polarization purity does not affect energy harvesting in a real-world multi-path environment.

D. Capacitor Charging, PMIC-Integration, and Powering a Bluetooth Wireless Sensor Node

In many real-world applications, the instantaneous DC power requirement of a load will be higher than the harvested power from a rectenna/RFEH surface. Therefore, an energy storage capacitor [44], supercapacitor [45], or battery [46], will

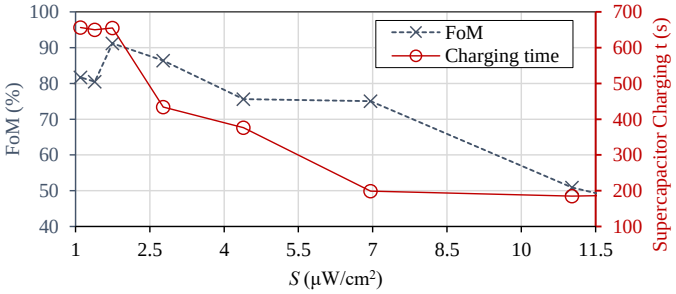

Fig. 13. Measured charging time and FoM (up to 3 V) for a 22 mF supercapacitor directly connected to the surface's output.

be required. It was previously shown that for S >1 μW/cm^2, a direct connection between the rectifier and a supercapacitor yields higher PCE than when using DC-DC converters [45].

The proposed surface's output is connected directly to a commercial 22 mF supercapacitor (FG0H223ZF) with a 5.5 V rating. The supercapacitor was charged at varying S values at which a 3 V DC potential can be reached, to enable the supercapacitor to directly power off-the-shelf components without stepping up. The average charging power $P_{\mathrm{DC,C}}$ is calculated as

$$P_{\mathrm{DC,C}} = \frac{CV^2}{2} \times \frac{1}{t_{\mathrm{charge}}} \tag{6}$$

where C is the capacitance, V is the capacitor's potential, and t_{charge} is the charging time. The FoM is then calculated using the (5) and the averaged $P_{\mathrm{DC-C}}$. Fig. 13 shows the FoM and the time taken to reach an approximately 3 V potential (i.e. 99 mJ) in the supercapacitor for varying S. It can be observed that the RFEH surface could generate the required potential for inputs as low as 1 μW/cm^2, in approximately eleven minutes (660 s) of charging. This energy can be directly used to power a Bluetooth Low Energy (BLE) Wireless Sensor Node (WSN) for over 100 s [25], indicating the suitability of the proposed surface for intermittently powering WSNs with a duty cycle of at least 10% from a 1 μW/cm^2 input.

At lower S values, the voltage needs to be stepped up. In most RF energy harvesting applications, a boost converter is required to enable the rectenna to power real-world systems [4], [15]. A Texas Instruments (TI) BQ25504 PMIC, widely used for its very low start-up voltage and quiescent current [18], [44], is used to boost the output voltage of the proposed surface. S was swept to identify the minimum power density required to start the BQ25504. The minimum S is found to be 0.25 μW/cm^2; the voltage charging curve of the BQ25504 is shown in Fig. 14. A period of 370 s is required to charge the 100 μF electrolytic capacitor, integrated with the BQ25504, to 4.2 V.

We then experimentally demonstrate that this configuration can supply a real-world load. A low-power BLE WSN based on the TI CC2640R2F Arm System on Chip (SoC) with an integrated 2.4 GHz BLE transceiver is programmed to advertise at 0 dBm transmitted power with a 100 ms duty-cycle. In addition, the Arm microcontroller also wakes up at a 30 ms interval, which emulates sensing functionalities. In addition to the active power consumption, the SoC requires a

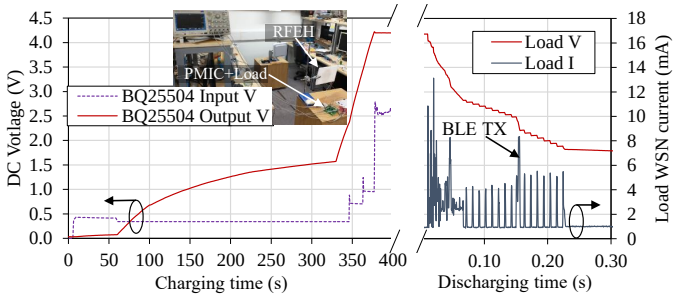

Fig. 14. Measured charging voltage curves of the BQ25504's 100 µF capacitor at S=0.25 µW/cm^2, along with the current drawn by the Bluetooth WSN.

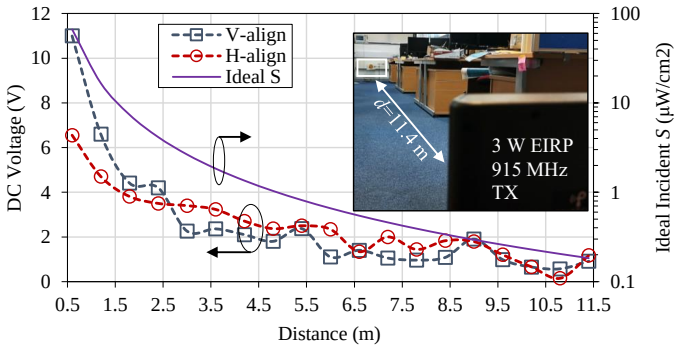

Fig. 15. Measured DC voltage output at varying distance from a 3 W 915 MHz V-LP Powercast source for vertical and horizontal surface orientation, at θ=φ=0°.

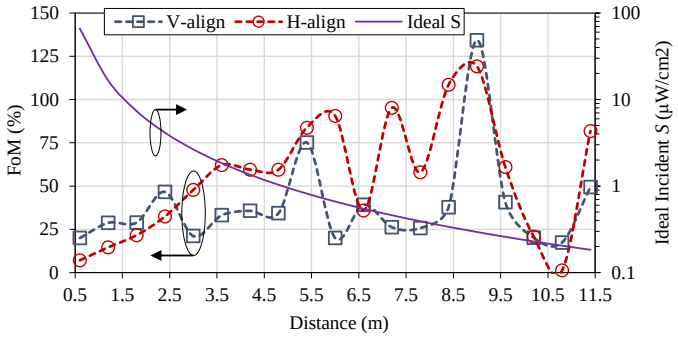

Fig. 16. Measured RFEH FoM, using the physical area (5), at varying distance from a 3 W 915 MHz V-LP Powercast source for vertical and horizontal surface orientation, at θ=φ=0°.

substantial start-up time of nearly 60 ms at a 1 mA current draw. Once the "power-good" indicator of the BQ25504 rises, indicating that the PMIC has successfully boosted the RFEH surface's output to the required 4.2 V potential, the capacitor is discharged into the BLE WSN. The current draw of the WSN, on the secondary axis of Fig. 14, demonstrates that the WSN has completed its start-up period and performed one BLE advertisement, which can be detected by a gateway far from the WSN. Should a longer WSN runtime be required, the 100 µF capacitor can be replaced with a larger model.

Compared to previous rectennas integrated with the same PMIC, the proposed RFEH surface achieves an unprecedented sensitivity, powering the BQ25504 from S=0.25 µW/cm^2. The lowest S demonstrated to date, powering the BQ25504, is 0.6 µW/cm^2 for a 3D reflector-backed compact dipole [4]. The 2.4-fold improvement by the six-element tightly-coupled array is in line with the improvement over the single-rectenna element based on the same FDA design, in Fig. 9, and further demonstrates the suitability of the proposed RFEH surface in low-power WSN applications.

E. Real-World Testing with a COTS Powercast

Following the characterization using a known S, a real-world V-polarized source, a 915 MHz 3 W EIRP Powercast source, is used to test the RFEH surface at varying distance. The effects of polarization misalignment alongside multi-path effects and ground-reflection will be illustrated, following the observed low polarization purity in Fig. 12(a)). The distance between the Powercast and the surface was varied between 0.5 and 11.5 m, with both the transmitter and the RFEH surface placed 70 cm height off the ground. The measurements were performed twice, with the RFEH surface aligned vertically with the Powercast's microstrip antenna, and with the surface horizontally aligned, i.e. orthogonal to the LP vertical patch. Fig. 15 shows the measured voltage output as a function of the distance from the 3 W 915 MHz source.

The FoM of the RFEH surface at varying distance from the 3 W source is shown in Fig. 16. Under two meters, the FoM is primarily limited by the breakdown voltage of the diode, where S exceeds 5 µW/cm^2. As the distance increases, the FoM approaches 100%. The peak measured FoM exceeding 100% due to using the surface's finite area in (5), is in line with that measured using a fixed circularly-polarized power source with a varying CW input, previously seen in Fig. 8. This further validates the proposed surface's ability to harvest incident linearly-polarized radiation with an FoM over 100%.

The fluctuation in both Fig. 15 and 16, is due to the combined effect of multi-path reflections and the low polarization purity. To explain, when the secondary paths have a higher amplitude than the primary path due to constructive/destructive interference, the array harvests more power at $\theta \neq 0°$, which as seen in Fig. 12(a) could lead to the surface having a vertical polarization. Thus, at such distances, e.g. 7 to 8.5 m, the horizontally-aligned surface yields a higher DC output. Previously, a high-efficiency single-element rectennas has also been demonstrated with a similar low polarization purity, which can be advantageous in unpredictable environments, e.g. ambient energy harvesting [42]. This highlights the need for dual-polarization harvesting [2], [5], [8]. This can be achieved in an RFEH surface by having multiple sub-surfaces which are horizontally and vertically aligned, to ensure both LP components can be harvested.

F. Comparison with Previous Work

The proposed finite RFEH surface based on small rectenna elements is compared to state-of-the-art implementations in Table I. Compared to all surfaces and arrays other than [12], the proposed RFEH surface is the only multi-rectenna harvester to achieve an FoM exceeding 100%, owing to its effective harvesting aperture that is nearly twice its physical footprint. While [12] recently reported a surface with an

TABLE I
COMPARISON WITH OTHER LARGE-AREA ARRAY AND FINITE SURFACE RF ENERGY HARVESTERS.

Study	Architecture	Number of Elements	Fabrication	Frequency	Diode	1 V Sensitivity*	FoM at S	Element PCE (%)	Load Powered
This work	Complex-conjugate small FDA array (element ka=0.58)	6 (series voltage summation)	Single-sided copper on flexible polyimide (t=0.00015λ)	915 MHz	SMS7630-079lf	0.2 μW/cm^2 (w/o boost converter)	170% S=5 μW/cm^2; 100% at S=0.4 μW/cm^2; 90% at S=1.75 μW/cm^2 with supercap.	36% at −20 dBm; 72% at −5 dBm	1:10 resistor range$^{\#}$; 22 mF supercapacitor; PMIC + Bluetooth WSN at S=0.25 μW/cm^2
TMTT 2004 [7]	CP broadband spiral array	64	NR	2 to 18 GHz	SMS7630	NR	0.1% at 0.01 μW/cm^2; 20% at 70 μW/cm^2	NR	Resistor
AWPL 2012 [21]	Single reflector-backed complex-Z rectenna	1	RT/Duroid 6002	2.4 GHz	HSMS-2852[§]	−5 dBm	Not applicable; single rectenna element	40% PCE at −20 dBm†	Resistor
TMTT 2014 [10]	LP dual-band dipole array	20	Flexible Rogers Tralam	0.915 and 2.45 GHz	SMS7630	NR; 2.5 μW/cm^2 w/ boost converter	50% at 10 μW/cm^2; 40% at 1 μW/cm^2	40.7% at −17.4 at 915 MHz	1:3 resistor ; boost converter from S >2.5 μW/cm^2
TMTT 2017 [9]	Half-wavelength dipole array	9	Double-sided copper on RO4003	2.45 GHz	HSMS-2863[§] and HSMS-2864[§]	NR	74% at 250 μW/cm^2; <25% at S <25 μW/cm^{2†}	NR	Resistor
TMTT 2018 [47]	Frequency Selective Surface	9	Double-sided copper on RO4003C	2.45 GHz	HSMS-2863[§] and HSMS-2864[§]	NR	60% at 263 μW/cm^2; <10% at S <5 μW/cm^{2†}	5% at −5 dBm; 60% at 15 dBm†	Resistor
TAP 2019 [13]	Vivaldi-inspired surface	16	Double-sided copper on RT-5880	2.9 GHz	HSMS-2860[§]	NR	60 at 150 μW/cm^2†	NR	Resistor
TMTT 2019 [8]	Cross-dipole array	49	Double-sided copper on RO5880	3 GHz	HSMS-2860[§]	NR (likely >10 μW/cm^2‡)	74% at 177 μW/cm^2	NR	Resistor
TMTT 2019 [14]	Planar cross-dipoles (0.12λ spacing)	27	Double-sided copper on RO5880	3.2 GHz†	HSMS-2860[§]	NR, >20 μW/cm^{2‡}	76% at >40 μW/cm^2	NR	Resistor
TMTT 2020 [11]	Bow-tie complex-conjugate array	16	Screen printing on textiles	2–5 GHz	SMS7630	≈110 μW/cm^{2†}	32% at 100 μW/cm^2; <5% at 1 W/cm^{2†}	<50%†	Resistor
Opt. Mat. Lett. 2022 [12]	Absorbing metamaterial with a Fabry-Perot resonator backing	8	Copper on FR4 with Fabry-Perot resonator at λ/10	900 MHz	SMS7630	NR	110%† at 2.6 μW/cm^2; 140%† at 36.4 μW/cm^2; <60% w/o GND plane	NR	Resistor

NR: not reported; *Minimum S for a 1 V output; † estimated from the graphs; ‡ calculated from the efficiency; **simulated result; # >60% of peak PCE.
§ Obsolete device (not available for new designs)

FoM around 130% (24% lower than the proposed surface), this performance was achieved using a 3D Fabry-Perot-like structure which results in a more directional harvesting pattern. In addition, such complex 3D construction does not fit within the planar and two-dimensional nature of most RFEH surfaces and planar arrays [1]. Without its reflector backing, the FoM

of [12] drops to 60%, which may be attributed to the lower element gain and rectifier PCE.

In addition, the proposed surface exhibits a significant FoM improvement over the only other surface implemented on a low-cost flexible substrate [11], due to the optimal impedance matching between the antenna and the rectifier maximizing the PCE. It is noted that in most prior RFEH surfaces, the PCE of a single element was not characterized experimentally, and hence, it is not possible to directly compare the rectifiers. However, the rectenna/rectifier's high PCE, shown in Fig. 6, is in line with state-of-the-art single-element rectennas using the same diode [17], [32] as well as those based on other diode models and complex 3D rectennas [21] (included in Table I for completion). Finally, the high sensitivity of the proposed RFEH surface is showcased in a real-world WSN powering application, as well as directly charging a supercapacitor with an FoM approaching 100%. The proposed RFEH surface achieves a state-of-the-art sensitivity from a sub-1 GHz S=0.25 μW/cm^2 input, powering a BLE WSN using a commercial PMIC, making it a suitable proposition for future WSN applications. To explain, compared to the arrays in [7], [10], demonstrated in emulation powering a DC-DC boost converter from S >2.5 μW/cm^2, the proposed six-element surface can power the commercial boost converter from an input as low as 0.25 μ W/cm^2.

While the achieved high-sensitivity is obtained at a relatively low frequency of operation, with a 1.5× improvement over a state-of-the-art sub-1 GHz surface, the proposed design could be extended to other frequency bands such as 2.4 GHz. To explain, a high-sensitivity rectenna was previously demonstrated with a comparable efficiency to the proposed rectenna, at 2.4 GHz [21], showing that the same rectification efficiency could be achieved at higher frequencies. Furthermore, the use of reflectors [48], based on either Perfect Electrical Conductors (PECs) or Perfect Magnetic Conductors (PMCs) could yield further performance gains at higher frequencies through more directional broadside harvesting.

V. Conclusion

In this paper, a thin and flexible low cost and complexity RFEH surface was presented based on complex-conjugate electrically-small dipoles. Despite its simple construction and DC combining mechanism, the proposed six-element FDA array achieves an unprecedented voltage sensitivity and figure of merit relative to its physical area. It is demonstrated that electrically-small antennas with optimal rectifier co-design, matching network-free, can yield multi-element tightly-coupled harvesters with an effective harvesting aperture exceeding their physical size, significantly improving their DC output compared to a single rectenna element. The proposed array exhibits significant performance improvements over existing 2D RFEH surfaces in the form of:

- a near-100% FoM improvement over other 2D surfaces;
- resistance compression-like response leading to a maintained output of over 60% of the peak power across a 1:10 load ratio;
- an ability to charge a supercapacitor with a high FoM and low charging times up to a 3 V potential from S>1 μW/cm^2;
- an unmatched sensitivity, powering a commercial PMIC and a Bluetooth WSN from power densities as low as 0.25 μW/cm^2;

It is expected that this work will motivate the integration of RFEH surfaces and tightly-coupled arrays, as opposed to individual rectennas or large arrays, in future WSN applications.

Acknowledgment

The data supporting this article is accessible from DOI: 10.5525/gla.researchdata.1312.

References

[1] E. Kwiatkowski, J. A. Estrada *et al.*, "Broadband RF Energy-Harvesting Arrays," *Proceedings of the IEEE*, vol. 110, no. 1, pp. 74–88, 2022.

[2] M. Wagih, A. S. Weddell, and S. Beeby, "Rectennas for RF Energy Harvesting and Wireless Power Transfer: a Review of Antenna Design [Antenna Applications Corner]," *IEEE Antennas Propag. Mag.*, vol. 62 no. 5, pp. 95 – 107, 2020.

[3] X. Gu, S. Hemour, and K. Wu, "Far-Field Wireless Power Harvesting: Nonlinear Modeling, Rectenna Design, and Emerging Applications," *Proceedings of the IEEE*, vol. 110, no. 1, pp. 56–73, 2022.

[4] A. Okba, A. Takacs, and H. Aubert, "Compact rectennas for ultra-low-power wireless transmission applications," *IEEE Trans. Microw. Theory Techn.*, vol. 67, 5, pp. 1697 – 1707, 2019.

[5] M. Wagih, A. S. Weddell, and S. Beeby, "Omnidirectional Dual-Polarized Low-Profile Textile Rectenna with over 50% Efficiency for Sub-μW/cm^2 Wearable Power Harvesting," *IEEE Transactions on Antennas and Propagation*, vol. 69, no. 5, pp. 2522–2536, 2021.

[6] B. Clerckx, A. Costanzo *et al.*, "Wireless Power Transmission: From Far Field to Near Field," *IEEE Microw. Mag.*, vol. 19, 6, pp. 69 – 82, 2018.

[7] J. Hagerty, F. Helmbrecht *et al.*, "Recycling ambient microwave energy with broad-band rectenna arrays," *IEEE Trans. Microw. Theory Techn.*, vol. 52, 3, pp. 1014 – 1024, 2002.

[8] A. Z. Ashoor and O. M. Ramahi, "Polarization-Independent Cross-Dipole Energy Harvesting Surface," *IEEE Trans. Microw. Theory Techn.*, vol. 67 no. 3, pp. 1130 –1137, 2019.

[9] F. Erkmen, T. S. Almoneef, and O. M. Ramahi, "Electromagnetic Energy Harvesting Using Full-Wave Rectification," *IEEE Trans. Microw. Theory Techn.*, vol. 65, 5, pp. 1843 – 1851, 2017.

[10] Z. Popovic, S. Korhummel *et al.*, "Scalable rf energy harvesting," *IEEE Transactions on Microwave Theory and Techniques*, vol. 62, no. 4, pp. 1046–1056, 2014.

[11] J. A. Estrada, E. Kwiatkowski *et al.*, "An RF-Harvesting Tightly-Coupled Rectenna Array Tee-Shirt with Greater than Octave Bandwidth," *IEEE Trans. Microw. Theory Techniq.*, vol. 68 no. 9, pp. 3908 – 3919, 2020.

[12] C. Fowler, S. Silva *et al.*, "High efficiency ambient RF energy harvesting by a metamaterial perfect absorber," *Opt. Mater. Express*, vol. 12, no. 3, pp. 1242–1250, Mar 2022.

[13] T. S. Almoneef, F. Erkmen *et al.*, "A New Approach to Microwave Rectennas Using Tightly Coupled Antennas," *IEEE Trans. Antennas Propag.*, vol. 66, 4, pp. 1714 – 1724, 2018.

[14] A. Z. Ashoor, T. S. Almoneef, and O. M. Ramahi, "A planar dipole array surface for electromagnetic energy harvesting and wireless power transfer," *IEEE Transactions on Microwave Theory and Techniques*, vol. 66, no. 3, pp. 1553–1560, 2018.

[15] J. Bito, R. Bahr *et al.*, "A Novel Solar and Electromagnetic Energy Harvesting System With a 3-D Printed Package for Energy Efficient Internet-of-Things Wireless Sensors," *IEEE Trans. Microw. Theory Techn.*, vol. 65 no. 5, pp. 1831 – 1842, 2017.

[16] V. Palazzi, J. Hester *et al.*, "A Novel Ultra-Lightweight Multiband Rectenna on Paper for RF Energy Harvesting in the Next Generation LTE Bands," *IEEE Trans. Microw. Theory Techn.*, vol. 66 no. 1, pp. 366 –379, 2018.

[17] M. Wagih, A. S. Weddell, and S. Beeby, "High-Efficiency Sub-1 GHz Flexible Compact Rectenna based on Parametric Antenna-Rectifier Co-Design," in *2020 IEEE/MTT-S International Microwave Symposium (IMS)*, 2020.

[18] J. Bito, J. G. Hester, and M. M. Tentzeris, "Ambient RF Energy Harvesting From a Two-Way Talk Radio for Flexible Wearable Wireless Sensor Devices Utilizing Inkjet Printing Technologies," *IEEE Trans. Microw. Theory Techn.*, vol. 63, 12, pp. 4533–4543, 2015.

[19] M. Wagih, A. S. Weddell, and S. Beeby, "Meshed High-Impedance Matching Network-Free Rectenna Optimized for Additive Manufacturing," *IEEE Open Journal of Antennas and Propagation*, vol. 1, pp. 615 – 626, 2020.

[20] M. Wagih, G. S. Hilton *et al.*, *IEEE Transactions on Antennas and Propagation*.

[21] H. Sun, Y. xin Guo *et al.*, "Design of a High-Efficiency 2.45-GHz Rectenna for Low-Input-Power Energy Harvesting," *IEEE Antennas Wireless Propag. Lett.*, vol. 11, pp. 929–932, 2012.

[22] J. Diao, L. Liu, and K. F. Warnick, "An intuitive way to understand mutual coupling effects in antenna arrays using the poynting streamline method," *IEEE Transactions on Antennas and Propagation*, vol. 67, no. 2, pp. 884–891, 2019.

[23] C. A. Balanis, "Antenna Theory: Analysis and Design. Third Edition," *Wiley Interscience*, pp. 84 – 85, 2005.

[24] W. Lin, R. W. Ziolkowski, and J. Huang, "Electrically small, low-profile, highly efficient, huygens dipole rectennas for wirelessly powering internet-of-things devices," *IEEE Transactions on Antennas and Propagation*, vol. 67, no. 6, pp. 3670–3679, 2019.

[25] M. Wagih, N. Hillier *et al.*, "Textile-based radio frequency energy harvesting and storage using ultra-compact rectennas with high effective-to-physical area ratio," in *2021 IEEE 20th International Conference on Micro and Nanotechnology for Power Generation and Energy Conversion Applications (PowerMEMS)*, 2021, pp. 32–35.

[26] H. A. Wheeler, "The radiansphere around a small antenna," *Proceedings of the IRE*, vol. 47, no. 8, pp. 1325–1331, 1959.

[27] M. Mi, M. Mickle *et al.*, "Rf energy harvesting with multiple antennas in the same space," *IEEE Antennas and Propagation Magazine*, vol. 47, no. 5, pp. 100–106, 2005.

[28] W. Brown and J. Triner, "Experimental thin-film, etched-circuit rectenna," in *1982 IEEE MTT-S International Microwave Symposium Digest*, 1982, pp. 185–187.

[29] W. Lin and R. W. Ziolkowski, "Electrically Small Huygens CP Rectenna With a Driven Loop Element Maximizes Its Wireless Power Transfer Efficiency," *IEEE Trans. Antennas Propag.*, vol. 68 no. 11, pp. 540 – 545, 2020.

[30] G. Marrocco, "The art of UHF RFID antenna design: impedance-matching and size-reduction techniques," *IEEE Antennas Propag. Magazine*, vol. 50, 1, pp. 66 – 79, 2008.

[31] C. H. P. Lorenz, S. Hemour *et al.*, "Breaking the Efficiency Barrier for Ambient Microwave Power Harvesting With Heterojunction Backward Tunnel Diodes," *IEEE Trans. Microw. Theory Techn.*, vol. 63, 12, pp. 4544 – 4555, 2015.

[32] S.-E. Adami, P. Proynov *et al.*, "A Flexible 2.45-GHz Power Harvesting Wristband With Net System Output From -24.3 dBm of RF Power," *IEEE Trans. Microw. Theory Techn.*, vol. 66 no. 1, pp. 380–395, 2018.

[33] C. R. Valenta and G. D. Durgin, "Harvesting Wireless Power: Survey of Energy-Harvester Conversion Efficiency in Far-Field, Wireless Power Transfer Systems," *IEEE Microw. Mag.*, vol. 15, 4, pp. 108–120, 2014.

[34] C. R. Paul, *Analysis of Multiconductor Transmission Lines, 2nd Edition*. Wiley-IEEE Press, 2007.

[35] M. Wagih, G. S. Hilton *et al.*, "Broadband Millimetre-Wave Textile-based Flexible Rectenna for Wearable Energy Harvesting ," *IEEE Trans. Microw Theory Techn*, vol. 68 no. 11, pp. 4960 – 4972, 2020.

[36] K. Niotaki, A. Georgiadis *et al.*, "Dual-Band Resistance Compression Networks for Improved Rectifier Performance," *IEEE Transactions on Microwave Theory and Techniques*, vol. 62, no. 12, pp. 3512–3521, 2014.

[37] C. Song, Y. Huang *et al.*, "Improved ultrawideband rectennas using hybrid resistance compression technique," *IEEE Transactions on Antennas and Propagation*, vol. 65, no. 4, pp. 2057–2062, 2017.

[38] R. Gutmann and J. Borrego, "Power combining in an array of microwave power rectifiers," *IEEE Transactions on Microwave Theory and Techniques*, vol. 27, no. 12, pp. 958–968, 1979.

[39] A. Eid, J. Hester, and M. M. Tentzeris, "A Scalable High-Gain and Large-Beamwidth mm-Wave Harvesting Approach for 5G-powered IoT," in *2019 IEEE MTT-S International Microwave Symposium (IMS)*, 2019.

[40] M. Wagih, A. Komolafe *et al.*, "Broadband compact substrate-independent textile wearable antenna for simultaneous near- and far-field wireless power transmission," *IEEE Open Journal of Antennas and Propagation*, vol. 3, pp. 398–411, 2022.

[41] S. Ladan, A. B. Guntupalli, and K. Wu, "A High-Efficiency 24 GHz Rectenna Development Towards Millimeter-Wave Energy Harvesting and Wireless Power Transmission," *IEEE Trans. Circuits And Systems*, vol. 61, 12, pp. 3358 – 3366, 2014.

[42] C. Song, Y. Huang *et al.*, "A High-Efficiency Broadband Rectenna for Ambient Wireless Energy Harvesting," *IEEE Trans. Antennas Propag.*, vol. 63, 8, pp. 3486–3495, 2015.

[43] N. Shinohara and H. Matsumoto, "Dependence of dc output of a rectenna array on the method of interconnection of its array elements," *Electrical Engineering in Japan*, vol. 125, no. 1, pp. 9–17, 1998.

[44] F. Moreno-Cruz, V. Toral-López *et al.*, "Dual-Band Store-and-Use System for RF Energy Harvesting With Off-the-Shelf DC/DC Converters," *IEEE Internet of Things Journal*, vol. 8, no. 5, pp. 3678–3688, 2021.

[45] M. Wagih, N. Hillier *et al.*, "Rf-powered wearable energy harvesting and storage module based on e-textile coplanar waveguide rectenna and supercapacitor," *IEEE Open Journal of Antennas and Propagation*, vol. 2, pp. 302 – 314, 2021.

[46] W. Zhao, K. Choi *et al.*, "A radio-frequency energy harvesting scheme for use in low-power ad hoc distributed networks," *IEEE Trans. Circuits And Systems*, vol. 59 no. 9, pp. 573 – 577, 2012.

[47] F. Erkmen, T. S. Almoneef, and O. M. Ramahi, "Scalable electromagnetic energy harvesting using frequency-selective surfaces," *IEEE Transactions on Microwave Theory and Techniques*, vol. 66, no. 5, pp. 2433–2441, 2018.

[48] M. Wagih, A. S. Weddell, and S. Beeby, "Analyzing and maximizing the power harvesting efficiency of a textile rectenna through reflector-based shielding," in *2021 15th European Conference on Antennas and Propagation (EuCAP)*, 2021, pp. 1–5.

Mahmoud Wagih (GS'18, M'21) received his B.Eng. (Hons.) in September 2018, and his Ph.D. on rectenna design in April 2021, both in Electrical and Electronic Engineering from the University of Southampton.

He is currently a Proleptic Lecturer (Assistant Professor) and UK IC Research Fellow, at the University of Glasgow, U.K. His interests broadly cover antennas and microwave technologies for sustainable electronics, and has over 60 refereed publications.

Dr. Wagih is a Senior Member of URSI and an affiliate member of the IEEE Microwave Theory & Techniques Technical Committees TC-25 and TC-26. He was the recipient of the Best Undergraduate Project Prize, School, Best in Faculty Doctoral Research Award, and the Dean's Award for Early Career Researchers, in 2018-2021, at the University of Southampton. He received the Best Student Paper Award at the IEEE Wireless Power Transfer Conference, 2019, the Best Oral Presentation Award at PowerMEMS, 2019, the IEEE MTT-S Best 3MT Presentation Prize (second place) at the IEEE Microwave Week, 2020, the Best Paper Award at PowerMEMS, 2021, and the EurAAP Best PhD in Antennas and Propagation "Per-Simon Kildal Award", 2022, and was a U.K. TechWorks Young Engineer of the Year finalist, in 2021.

Steve Beeby (FIEEE) received the B.Eng. (Hons.) degree in mechanical engineering from the University of Portsmouth, U.K., in 1992, and the Ph.D. degree in MEMS resonant sensors from the University of Southampton, U.K., in 1998.

He is currently the Director of the Centre for Flexible Electronics and E-Textiles and leads the U.K.'s E-Textiles Network. He is currently leading three U.K. funded research projects and has received over £20 million research funding. He is a co-founder of Perpetuum Ltd., a University spin-out based upon vibration energy harvesting formed in 2004, Smart Fabric Inks Ltd., and D4 Technology Ltd. He has given over 30 plenary/keynote/invited talks and has over 350 publications and an h-Index of 56. His current research interests focus on energy harvesting, e-textiles and the use of energy harvesting in wearable applications.

Prof. Beeby was the recipient of two prestigious EPSRC Research Fellowships to investigate the combination of screen-printed active materials with micromachined structures and textiles for energy harvesting and was also awarded a Personal Chair in 2011. He has most recently been awarded a prestigious RAEng Chair in Emerging Technologies in E-textile Engineering.